J Mater Sci (2010) 45:4115–4125
DOI 10.1007/s10853-010-4500-x

Comparison between the process–structure–property relationships of silica foams prepared through two different processing routes

Sarika Mishra · R. Mitra

Received: 30 November 2009 / Accepted: 7 April 2010 / Published online: 21 April 2010

Abstract Cellular silica with improved framework, crosslinking, and stability properties are desirable for applications in thermal insulation. A process for the preparation of cellular silica foam with interconnected cells with tailored porosity and pore size distribution has been attempted. The silica foams have been prepared through two different methods; surfactant- and particle-based stabilization. The silica foams prepared through two different processes namely surfactant-stabilized foams (SSF) and particle-stabilized foams (PSF) have exhibited a wide range of differences in their structure which in turn have shown to affect the final properties of the foam. The cell size distributions in SSF (89 vol% porosity) and PSF (85 vol% porosity) have been found in the range of 50–250 μm (monomodal) and 4–10 μm and 50–100 μm (bimodal), respectively, whereas the cell counts of both have been found in close proximity. The microstructure of both the sintered SSF as well as PSF samples foams have shown an open and interconnected porosity with the permeability of both in the region of $\sim 10^{-8}$ m^2. The mechanical (compressive) strength and Young's modulus of the PSF are a third of that in SSF. The structure–property relationship of both the SSF and PSF and their comparison have been discussed.

S. Mishra (✉)
Non Ferrous Materials Technology Development Centre,
P.O. Kanchanbagh, Hyderabad 500058, India
e-mail: uptecsarika@rediffmail.com

R. Mitra
Indian Institute of Technology, Kharagpur 721302, India

Introduction

Ceramic foams are known to have high permeability, high specific surface area, excellent insulating characteristics, high refractoriness, chemical resistance, and long life in severe environments due to their high porosity, well-developed surface pores, and three-dimensional network pore structure [1–3]. Those characteristics enable ceramic foams to be widely used in industrial fields as filters for contaminated hot gas purification [3, 4], catalyst carriers [5, 6], refractories [3, 7], thermal insulators [3, 8], and biomedical substitutes with skeletal and dental functions [1, 8]. Several methods, such as polymeric sponge method [3, 9, 10] and foaming method [3, 11] have been commonly utilized to prepare ceramic foams. Among these, the foaming method has an advantage in that it can conveniently control the pore structure of ceramic foams by artificially controlling the foam volume expansion ratio (ERFV), which is defined as the ratio of volume of the foamed slurry to that of original. Therefore, developing highly stabilized three-phase (solid–liquid–gas) foams is the first and most critical step to prepare suitable ceramic foams [11–13]. In many cases, such a foaming process generates a high density of bubbles and disperses them in the foam slurry. The bubbles are finally converted into pores between solid particles in the ceramic foam through shaping and heating processes. Therefore, pore-related parameters (porosity, pore size, and pore morphology) can significantly affect the global characteristics of the ceramic foams, such as the specific surface area, water absorption, surface roughness, permeability, and foam destabilization. Pore size in particular is one of the most important properties in determining the practical applications of ceramic foam [12].

It is, in principle, possible to retard such process of destabilization by increasing the viscosity of the medium and kinetically stabilize the foam [14]. In such a case, the foam with a distribution of air bubbles is produced as a result of the interplay of surface tension and viscosity. While the surface tension promotes the bubble formation, the viscosity impedes bubble growth and subsequent collapse [15–18]. Therefore, the most critical issue in the direct foaming method is the approach used to stabilize the air bubbles incorporated within the initial suspension or liquid media. The foams have been stabilized using either the surfactants or using surface-modified particles. Based on the approach used for foam stabilization accompanying the direct foaming process, the porous products are classified as: surfactant-stabilized foams (SSF) and particle-stabilized foams (PSF) [19–26]. The process of surfactant stabilization involves the addition of long-chain surfactants into the ceramic slurries, which are then subjected to effective air entrainment for producing ceramic foams.

In the particle stabilization route, the solid particles with tailored surface chemistry have been shown to efficiently stabilize gas bubbles upon adsorption at the air–water interface [15–19, 27]. Particles adsorbed at the gas–liquid interface impede the destabilization mechanisms responsible for bubble coalescence for several days, as opposed to the few minutes typically required for the collapse of foams prepared with long-chain surfactants. For the fabrication of PSF, the attachment of colloidal particles at the air–water interface is promoted by deliberately changing the wettability of the particle upon adsorption of short-chain amphiphilic (surfactant) molecules on the surface [28]. The amphiphiles initially added to the suspension render the particle partially hydrophobic by being adsorbed with its polar anchoring group on the surface and leaving a short hydrophobic tail (up to six carbons) in contact with the aqueous phase [15–19]. In a recent study on PSF [14], the α-alumina powder particles (mean size ~200 nm) hydrophobized by short chain amphiphile (<C8) has been successfully used for stabilization of foams. The study has shown that the concentration of amphiphile required to render the particles sufficiently hydrophobic so that these are adsorbed at the air–water interface decreases significantly with increasing C-chain (tail) length of amphiphile molecule as the increasing tail length increases the hydrophobic nature of amphiphile.

The present study has been undertaken to arrive at a simple method of processing large size porous silica tiles, by applying the concept of particle stabilization of foams with the help of long-chain amphiphilic molecules attached to hydrophobized silica particles. This paper focuses on the development of porous silica through both surfactant stabilization and particle stabilization routes. Both the foams namely SSF and PSF have been compared in terms of their stability and process-structure-property relationships.

Experimental procedure

Raw materials

The raw materials used in the study include fused silica powder ($d_{50} = 20$ μm, Industrial grade), alumina powder (d_{50} ~0.70 μm, surface area ~7 m^2/g, Industrial grade), cetyl trimethyl ammonium bromide or CTAB (98% pure, CR grade, S.D. Fine Chemicals Ltd.) as cationic dispersant, and PVA (molecular wt = 1,25,000, LR grade, Fischer), sucrose (LR grade, S.D. Fine Chemicals Ltd.), as binders. In addition, isopropanol (99% pure, S.D. Fine Chemicals Ltd., LR grade), an organic solvent which reduces the surface tension of water in aqueous suspensions was used in the study to improve the wetting behavior of the powder particles in particle-based stabilization method.

Slurry preparation and processing

Fused silica powder along with 5 wt% fine alumina and 0.05% cetyl trimethyl ammonium bromide was ball milled in water using alumina milling media in 1:1 ratio for 100 h in order to achieve a particle size of ~5 μm and this partially hydrophobized pretreated powder was used for the making both the foams. The detailed procedure for the slurry preparation and further slurry processing for the preparation of SSF [29] and PSF [30] are described elsewhere.

Optimization of processing parameters on foam properties in PSF

Solids loading

Experiments were carried out in test tubes with different levels of solid loading starting with 1–5 wt% of fused silica powder suspended in 10 mL liquid medium. The liquid comprised isopropanol and water in 1:10 ratio along with PVA and sucrose. In all the cases, vigorous mechanical agitation of the suspensions for 10–15 min set the foam at the top of the suspension leaving a clear solvent zone below. The test tubes containing the suspensions were carefully examined for studying the settling behavior of the powder. The extent of slurry stabilization, in principle, was determined from the amount of the powder particles settling at the bottom. The photograph depicting the experimental set-up showing the test tubes with 1, 2, and 3 wt% fused silica powder in the suspension is shown in Fig. 1.

Isopropanol addition

To determine the wetting behavior of partially hydrophobic silica particles, a series of test tube experiments were

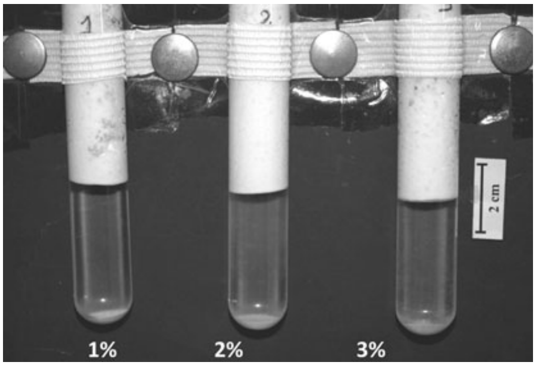

Fig. 1 Photograph of the test-tube experiment showing the effect of solids loading on stability of suspensions

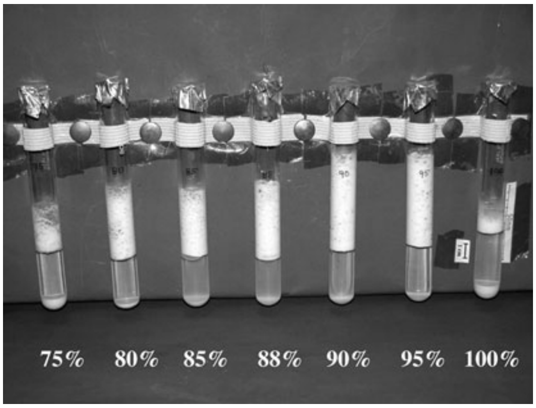

Fig. 2 Photograph depicting the set-up used for test-tube experiments for studying the effect of isopropanol on the wetting behavior of the silica powder particles in isopropanol–water mixture. The label shows the percentage volume fraction of water in the mixture in each of the test-tube

performed, in a way similar to that for solids loading (Fig. 2). For each experiment, 1 g of fused silica powder was added exactly at the top of the water–isopropanol mixture layer and its wetting time was carefully examined with the help of a stop watch from the time of powder addition to either settling of the powder at the bottom, or attainment of a layer of powder at the liquid-air interphase. The water to isopropanol ratio was varied from 75:1 to 100:1, and the volume fraction of water was plotted against the wetting time.

Characterizations

Rheology

The rheological behavior of the silica suspensions were examined using a rotary viscometer in parallel plate configuration (40 mm diameter, 1 mm gap) with a solvent trap (Model AR1000, TA Instruments, New Castle, DE). The measurements were performed at room temperature, RT (27 °C) at shear rates varying from 0.5 to 50 s^{-1} prior to the foaming step.

Density and shrinkage

The relative density was determined for each of the SSF and PSF foams in green as well as sintered stage, used in the study. The bulk density of the foam samples was calculated from the data on specimen mass and volume obtained using direct measurements. The theoretical density was calculated by applying the rule of mixtures to the volume fractions of the foam constituents. Subsequently, the relative density (ρ) was thus obtained by normalizing the bulk density with the theoretical density of the material. The linear and volume shrinkages upon drying were calculated by measuring the dimensions of the PSF samples before and after drying.

Permeability

The room temperature air permeability of sintered discs of SSF and PSF having dimensions of 25 × 25 × 8 mm size (each 3 samples) was determined by an in-house made experimental set-up. The experimental set-up was prepared following the standard procedure recommended in ASTM C 577-99 [31] for measuring the air pressure drop across the sample as a function of the gas flow rate.

For the permeability measurements, the foam samples were prepared by soaking them initially in resin and then cross-linking them at 130 °C for 10 min. It was then followed by cutting the samples carefully into 25 × 25 × 8 mm size blocks. The samples were then placed in the sample holder made up of aluminum metal, and secured in position with the help of rubber gasket. Argon gas from the source was made to flow through the foam sample and across it, and the pressure gradient across it was measured with the help of barometric gauges. In addition, the gas flow rate through the sample was determined with the help of rotameters. The two big size gas flow meters, each with a steel needle (scale range 0.16–1.57 CFM), were used to measure the flow rate for low density foam samples, whereas the two smaller size flow meters with plastic ball (scale range 0.015–0.150 CFM) were used to measure the gas flow rates for the foam samples with higher densities. Absence of gas leakage in the equipment was checked with water bubbles. Pressure drops were verified through repeated tests for each disc to check the reproducibility of the measurements.

For pore sizes <1 mm, the gas flow rate, Q, through a porous sample is related to the pressure drop, ΔP, across the length, L, by an expression (1) based on Darcy's law [32] as shown:

$$Q = \frac{K_D A \Delta P}{L\eta} \quad (1)$$

where A is cross-sectional area of sample, η is the viscosity of the flowing medium and K_D is the Darcy permeability coefficient.

X-ray radiography

The sintered foam panels of SSF and PSF were examined using X-Ray radiography (Philips Model No. MCC-40, West Germany, capacity 450 kV) operated at 85–90 kV for an exposure time of 60 s. The X-ray radiography was carried out as a tool for nondestructive testing in order to detect the defects within the samples.

Microstructure

Small vertical sections of the foam samples were impregnated with resin and subjected to curing at 130 °C for 15 min, in order to improve their handling strength. After curing, the resin impregnated foam samples were sectioned into round discs of 9.25 mm diameter and 2 mm height, and subjected to microstructural examination. The microstructures of sintered foam samples were studied using an optical microscope equipped with a digital camera (Biovis MV500 Image Acquisition, analysis software Biovismat Plus, Version 1.5) and scanning electron microscopy (SEM) (Leo 440i, UK).

The recorded SEM images of the silica foams were characterized using image analysis software (Image Tool, Version 3.0, University of Texas Health Science Center, San Antonio, TX). The image analysis was done on at least three micrographs for the estimation for pore count and size in SSF and PSF. In addition, the fracture surfaces generated through compression tests were examined using optical microscopy at low magnification (×6).

Pore size distribution

The pore size distribution in the sintered and drilled cylindrical samples (9.25 mm diameter) was estimated through mercury (Hg) intrusion porosimetry (Quantachrome Poremaster, version 4.01, Hg contact angle 140°, pore size detection range from 1 mm down to 3.5 nm). In this technique, the nonwetting liquid, mercury, is forced into pores of the sample [33, 34]. The pressure required to intrude mercury into a pore is given by the relation (2) known as the Washburn equation, as follows:

$$P = \frac{-4\gamma \cos\theta}{D} \quad (2)$$

where P is the pressure of mercury, γ is the surface tension of mercury, θ is the contact angle of mercury, and D is the diameter of the pore. Both the pressure on mercury and the decrease in volume of mercury due to intrusion were measured and the data was used to compute the average pore size, as well the net pore volume and size distribution.

Compressive strength

For compression tests, the resin-impregnated SSF and PSF samples (after curing of resin) were drilled using ultrasonic drilling machine to obtain cylindrical samples, having the dimensions of 9.25 mm diameter and 19–22 mm height. The finally machined resin impregnated samples were then subjected to heat treatment at 650 °C to remove the resin, which in turn leaves behind the silica foam intact. The foams were then compression tested using Instron 5501R Universal Testing Machine. Following the technique used by Brezny and Green [35], wooden spacers of 9.25 mm diameter and 6 mm height were fixed to both the flat ends of the cylindrical samples, so that load transfer to the samples was uniform. Further, the static elastic (Young's) modulus was estimated from the slope of the elastic part of the stress–strain curve. A total of 10 samples were tested in order to calculate the Weibull modulus from the experimental data.

Results and discussion

Effect of processing parameters on foam properties in PSF

The results of test tube experiments (each with 10 ml suspension) described earlier in "Solids loading" justify that 3 wt% (~13.3 vol%) solids loading is an optimum for preparation of the PSFs. On the other hand, the trial experiments involving vigorous mechanical agitation of the suspensions with different compositions (from experiment described in "Isopropanol addition"), have shown that the volume of the foam is the highest in the suspension with isopropanol-to-water ratio (IWR) of 1:9 with wetting time 27 min. Hence each of the PSF in this study has been processed using suspensions with IWR = 1:9. The detailed results on the optimization of processing parameters in PSFs are described elsewhere [30].

Rheology

In PSF, experiments involving vigorous shaking of the suspension with optimized composition for 10–15 min have shown 2–2.5-fold increase in its apparent volume. No further increase in the apparent volume could be observed for shaking periods exceeding 15 min, due to attainment of the saturation limit of foaming. Test tube experiment using

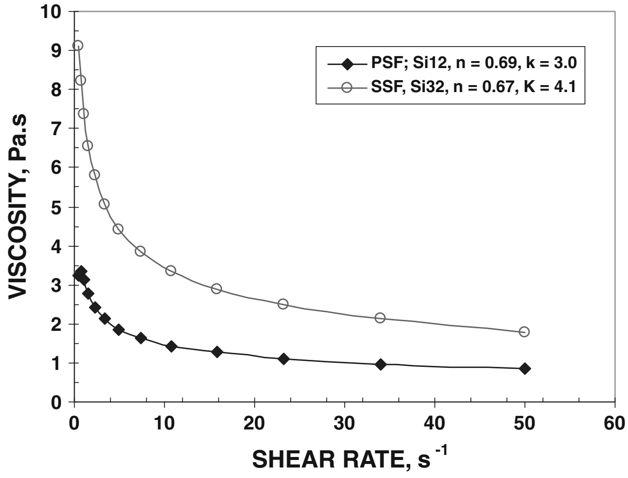

Fig. 3 Plots showing the variation of viscosity with shear rate for silica slurries in PSF and SSF at RT

the optimized composition (low solids loading of 13.3 vol%) has led to the formation of stable foamed suspension with a very low viscosity of <2 Pa s at 10 s^{-1} shear rate, as shown in Fig. 3. Although, the initial viscosity of the PSF suspensions remains very low, yet disproportionation and collapse of the final foam has not been observed. In fact, the foam obtained in this study has been found to be thick and stable for several days so that collapse and coalescence of air bubbles is inhibited.

The stability of air bubbles formed in the PSF is remarkable, when compared to that observed during preparation of SSF, as a few minutes are typically required for the collapse of the foam. Again, in case of the SSF, suspension having an optimum minimum solids loading of 30–35 vol%, and a viscosity of ~3.4 Pa s at a shear rate of 10 s^{-1} (Fig. 5) are desirable for their own stability and for stable foam. Thus, it may be inferred that both the solids loading and viscosity of suspensions used in preparation of SSF are greater than those corresponding to the PSF.

The mechanism proposed for the outstanding stability of the foams or use of the colloidal hydrphobized silica particles is based on the adsorption of the silica–amphiphile complex at the air–water interface of the gas bubbles [18, 19]. The energy required to desorb a particle–amphiphile complex from an air–water interface is orders of magnitude higher than what is needed to desorb a surfactant molecule from the interface [14, 20]. It suggests that hydrophobic silica particles attached to the air–liquid interface impede the coalescence of neighboring bubbles through steric hindrance and also form a coating layer on air bubbles due to the reduction in free energy on adsorption of the amphiphile molecule attached to the fused silica particles at the air–water interface. This phenomenon explains the mechanism inhibiting the shrinkage of some bubbles and expansion of others due to Ostwald ripening.

Direct observation for confirming the presence of hydrophobized silica particles at the air–water interface has not been carried out in this study. However, quite recently confocal microscopy [18] has been used to prove the role of complexes of silica particles and hexylamine in stabilization of the foam at the air–water interphase. For the purpose of confocal microscopy, fluorescent silica particles have been used by Gonzenbach et al. [14, 18]. As a similar procedure has been used for processing of PSF in the present study, the mechanism proposed above for the stability of foams is justified.

Density and shrinkage

Photographs of the green panels (or tiles) made from the silica-based PSF panels with dimensions of about 100 × 60 × 30 mm size and SSF-based suspensions are shown in Fig. 4. The density, porosity content, and shrinkages (linear and volume) of both the green and sintered bodies for SSF and PSF are listed in Table 1.

The densities of wet PSF have been measured as 0.524 ± 0.18 g/cc., while those of the green (dried condition) panels have been found as 0.358 ± 0.13 g/cc. The significant fall in density as well as high shrinkages observed on drying can be attributed to the higher volume of liquid adhering to the foam surface. In addition, the process for making SSF consistently yields a density of 0.368 ± 0.045 g/cc for wet foam samples and 0.248 ± 0.03 g/cc (RD = 0.11 ± 0.013) for the green bodies.

It has also been observed that the weight loss upon drying in PSF constitutes almost 40–50% of the sample weight. The

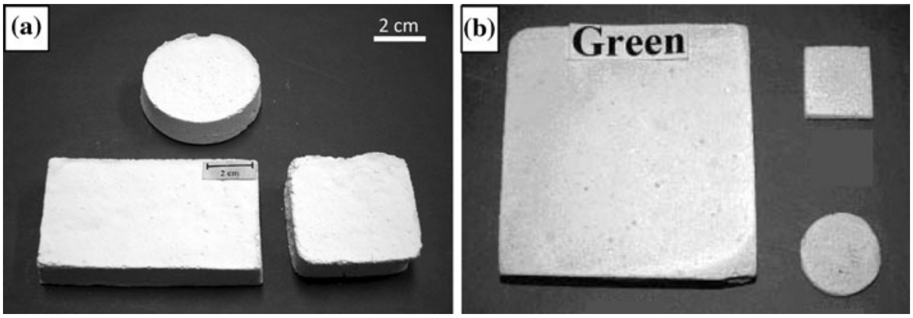

Fig. 4 Photographs of **a** sintered PSF panels of various shapes and sizes with 85 vol% porosity, and **b** green SSF samples, subjected to drying up to 110 °C. Photograph **b** is showing a typical 100 × 100 × 25 mm panel; a square disc and a round disc cut from the panel

Table 1 Density and shrinkage data for silica foam panels

	SSF	PSF
Green body characteristics		
Density (apparent/RD)	0.225–0.27 (0.10–0.12)	0.358 (0.16)
Linear drying shrinkage (%)	4	11
Volume shrinkage (%)	23	28
Sintered body characteristics		
Relative density	0.105	0.15
Porosity (vol%)	90.5	85
Sintering shrinkage (%)	Negligible	Negligible

significantly large weight loss during drying of the PSFs is due to a larger volume fraction of moisture content. But in both the cases, under optimized drying conditions, even 30 mm thick panels could be dried without cracking.

X-ray radiography

The sintered silica foams with square or circular cross sections were subjected to X-ray radiography in order to examine the density gradient (based on color contrast) within the foams. A photograph recorded using X-Ray radiographic investigation of the green PSF and SSF sample is shown in Fig. 5a, b, respectively.

Comparison of the radiographic images of foams (Fig. 5a, b) indicates that the images of foams with a higher volume fraction of porosity (SSF) appear brighter than the images of foams with higher density (PSF). The dried PSF samples have not shown any evidence of surface cracking throughout the sample, in spite of the removal of a large amount of liquid within the foam lamella, during the drying process. Usually, the presence of such a large amount of liquid leads to foam collapse in surfactant-stabilization based method.

Microstructure and permeability

Cell count

A typical optical micrograph of the sintered PSF and SSF sample with a relative density (RD) 0.15 and 0.11 is shown in Fig. 6a, b, respectively. Examination of the structure of the PSF and SSF samples, as shown in Fig. 6, indicates that nearly spherical cells are scattered throughout. Further, the cells in the PSF are open and interconnected, similar to those observed in case of SSF.

Measurement of the cell sizes using image analysis of several optical micrographs shows the presence of only larger cells with a mean size of ≈680 μm, so that the “cell count” is 8 ppi (pores per inch). It can be seen from the optical micrographs in Fig. 6, that a large volume fraction of the foam consists of cells smaller than the resolution limit of the optical microscopy technique. On the other hand, the SSF with RD = 0.11 show uniform cell sizes (∼50 μm), with an average cell count of ∼10 ppi.

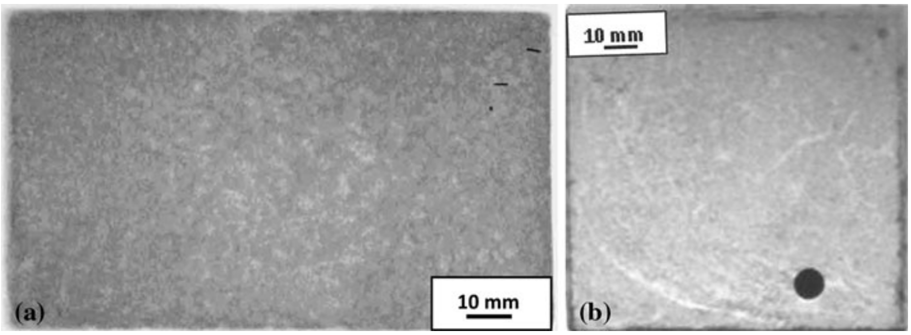

Fig. 5 X-ray radiographs of **a** a defect-free PSF tile (100 × 60 × 30 mm), and **b** SSF panel dried at 100 °C. An alumina ball of 8 mm diameter (as a reference) is shown in **b** as a *black round* feature

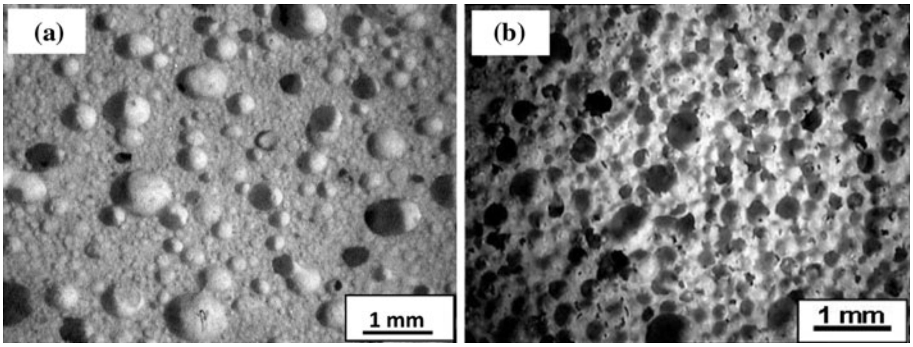

Fig. 6 Optical micrograph of **a** PSF with RD of 0.15, and **b** SSF with RD of 0.11

Scanning electron microscopy (SEM)

The microstructures of the PSF are shown in the SEM micrographs presented in Fig. 7. The SEM image of the PSF sample at lower magnification, presented in Fig. 7a, shows spherical cells, which are open, interconnected, and almost uniformly distributed. Visual examination of the SEM images suggests that a bimodal distribution of cells is present (e.g. Fig. 7a). The smaller and larger cell sizes in the bimodal distribution have been found to be in the range of 4–10 µm and 50–100 µm, respectively. Hence, it can be inferred on the basis of SEM studies, that majority of the cells in the PSF samples are much smaller than those found in the SSF (≈50–250 µm). However, larger cells with an average size of 680 µm observed using optical microscopy (Fig. 6) indicate that pore size distribution in the PSF is very wide. It can be seen from the Fig. 8b that the cell wall is porous and consists of very small pores (4–5 µm) in

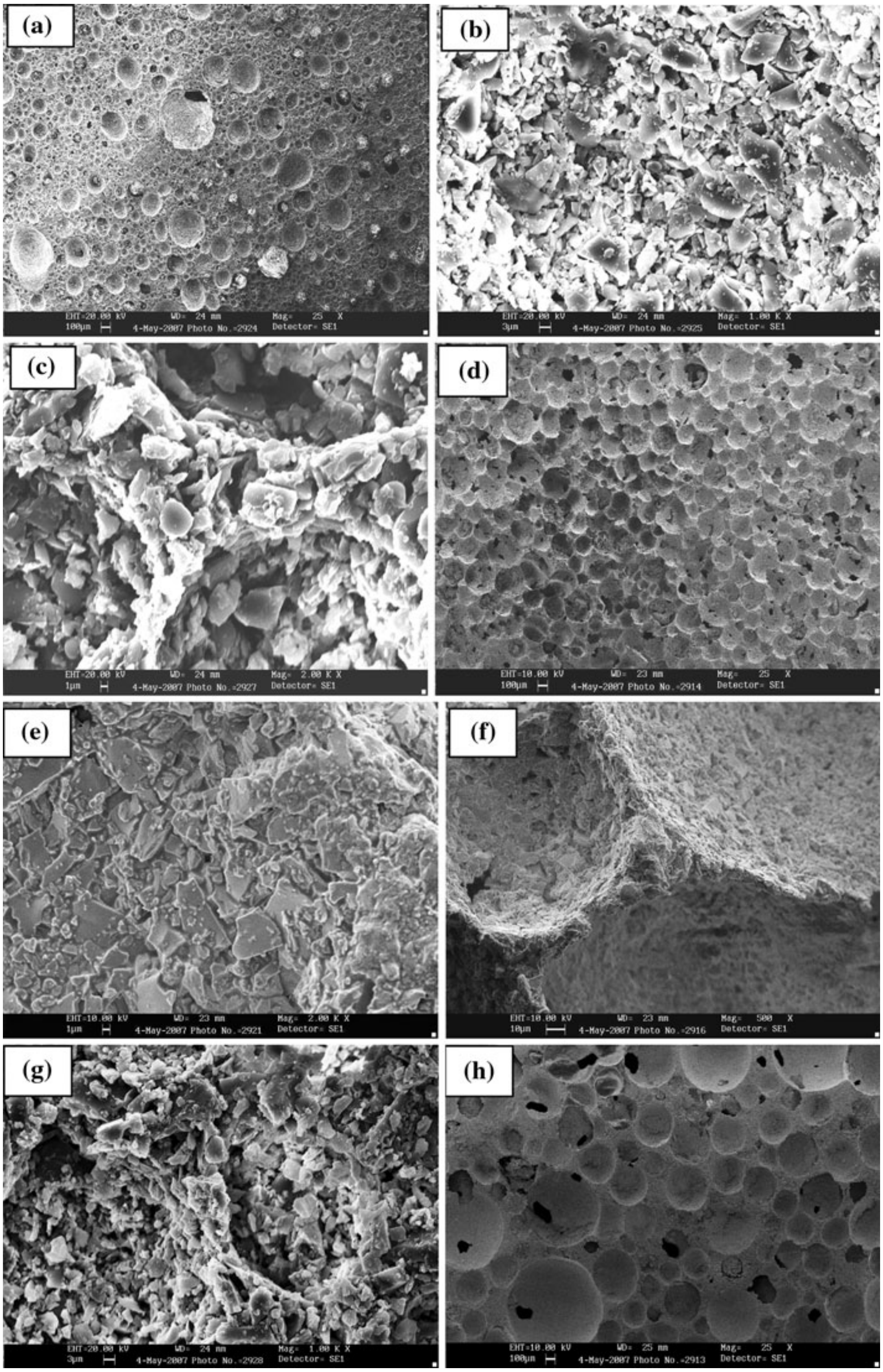

Fig. 7 SEM micrographs of silica foams showing: **a** spherical cells at low magnification in PSF; **b** bubble crest at high magnification showing densification in PSF; **c** a triangular strut shown at a higher magnification in PSF; **d** spherical cells at low magnification in SSF; **e** bubble crest at high magnification showing densification in SSF; **f** a triangular strut shown at a higher magnification in SSF; **g** cell wall at high magnification showing interconnections between the cells in PSF; and (**h**) low magnification micrograph of SSF showing interconnections between the cells

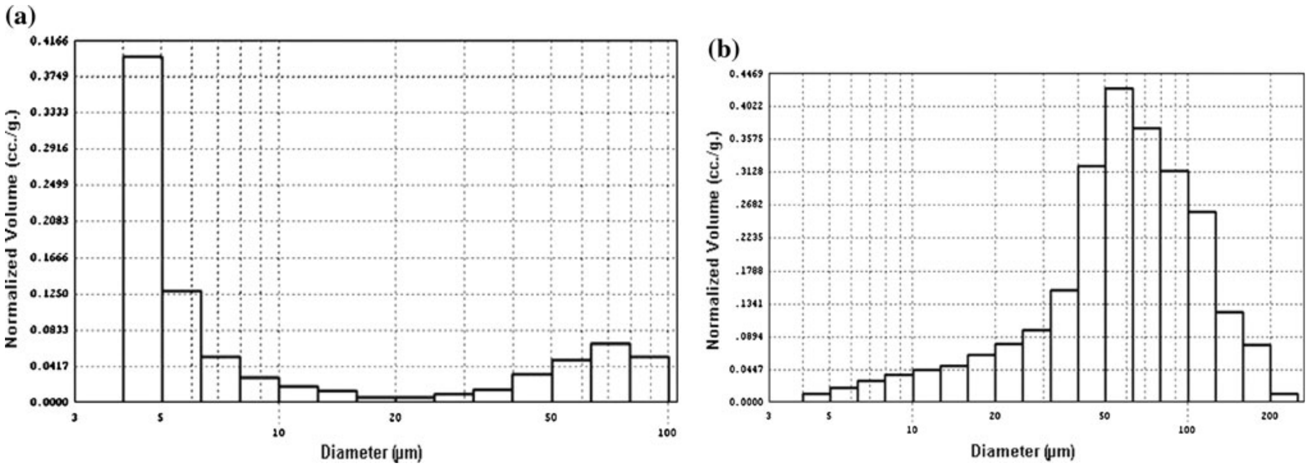

Fig. 8 Histogram of normalized cell volume per unit mass as a function of cell diameter for **a** PSF and **b** SSF

large volume fraction. The analysis carried out on SEM micrographs depicting the cell walls (bubble crest) (Fig. 7b) and triangular struts (Fig. 7c) region (to estimate the pore sizes of lower size) shows that the mean size of pores in these locations is ≈7 μm. Measurement of strut dimensions in the foams obtained using the particle stabilization methods (Fig. 7c) indicates the average strut wall thickness is ~1–2 μm.

In contrast, in SSF, the morphology of cells shows that the cells are nearly spherical and more uniformly distributed in the SSF foams with RD = 0.11 (Fig. 7d). The cell walls appear to be dense (absence of micropores), but the grains located in the cell walls are of different sizes and shapes (Fig. 7e). Measurements using the optical images (Fig. 7f) show that the average strut thickness is ~4–5 μm.

The use of surface-modified particles (in PSF) to stabilize the wet foam has decreased the lower limit of cell sizes to an average value of as low as 5 μm. Such small cell sizes result from the remarkable long-term stability achieved because of the reduction in pore surface energy through the irreversible adsorption of colloidal surfactant–silica complex (hydrophobized) at the air–water interface. Similar morphological features have been reported for alumina- and cordierite-based cellular solids using X-ray tomography images [36].

Permeability

In this study, the permeability of both the sintered SSF as well as PSF samples (25 × 25 × 8 mm) has been measured in the region of ~10^{-8} m^2.

Mercury porosimetry

Pore size distribution and surface area

Bar diagrams depicting the cell size distributions in the PSF measured through mercury porosimetry are shown in Fig. 8a, while the cumulative surface area of the cells is plotted against the cell diameter in Fig. 9a. Examination of

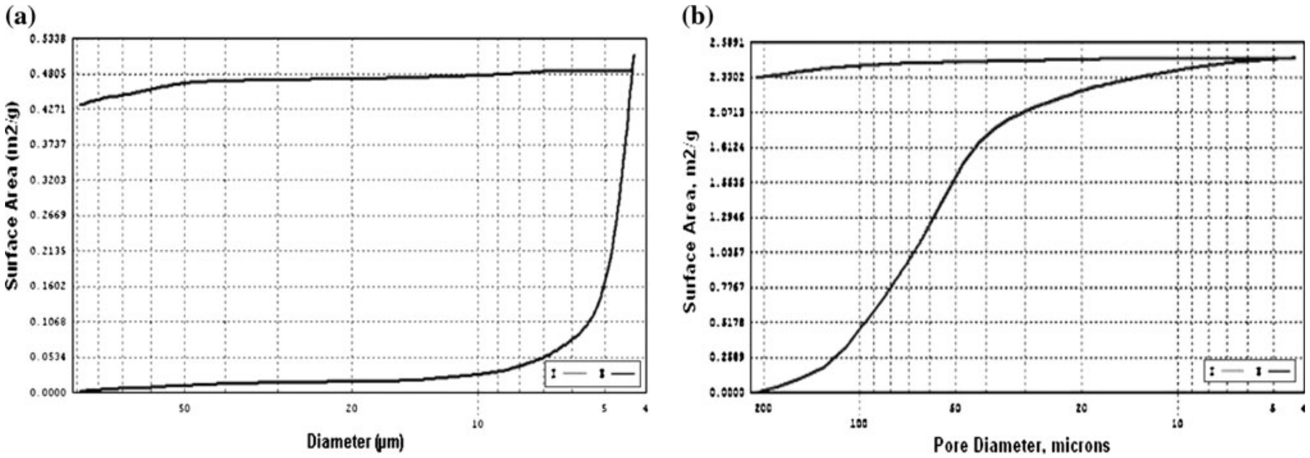

Fig. 9 Plot showing cumulative cell surface area per unit mass as a function of cell diameter for **a** PSF and **b** SSF

the data shown in Fig. 8 indicates that: (i) the highest volume fraction of cells lies in the range of 4–10 μm (mean cell size = 6.76 μm); (ii) the pore size distribution is bimodal with the larger pores having diameter in the range of 50–100 μm (mean cell size = 70 μm); (iii) the cumulative surface per unit mass of foam area corresponding to the cells with the highest volume fraction is 0.51 m^2/g; and (iv) the surface area corresponding to the mean cell sizes of 6.76 and 70 μm are 0.06 and 6.6×10^{-3} m^2/g, respectively.

Comparison of the mercury porosimetry results of the PSF with those of the foam obtained using the surfactant stabilization (SSF) indicates that there are two major differences: (i) the sizes of cells having the peak volume fraction in the PSF (~4–5 μm) is much less than those observed in the SSF (~50–250 μm) (Fig. 8b); and (ii) the cumulative surface area per unit mass of (0.51 m^2/g) the PSF is more than twice that (0.24 m^2/g) found for the cells with the highest volume fraction in SSF (Fig. 9b). The results of cumulative surface area measurements follow the presence of much finer cells in the PSF than in the SSF. The presence of bimodal distribution of cell sizes in the ceramic foams suggests that larger bubbles are formed in addition to the smaller ones during the foaming operation. The formation of larger bubbles in the PSF is perhaps due to the partial disproportionation (Ostwald ripening) process, which cannot be totally inhibited. The very small cells formed during the mechanical frothing (agitation) of suspension, come closer and coalesce within the foam lamella during drainage of liquid and lead to the formation of bubbles of larger sizes. The contact between the finer bubbles can be restricted through the increase in viscosity of initial suspension in the particle stabilization method with the increase in solids loading. In addition, the partial disproportionation and collapse of air bubbles in the wet PSF can be sterically hindered in order to attain a stable foamed suspension which in turn can result into PSF with an average smaller cell size with a narrow cell size distribution. However, this aspect has not been investigated in this study, as the attention is primarily on particle stabilization of foam. The above discussion leads to the inference that the method of particle stabilization needs to be supplemented by addition of additives which can provide promoting the steric hindrance to movement of air bubbles in wet foams in order to prevent their collapse or growth.

Mechanical behavior

The compressive strengths of the sintered PSF samples at the ambient temperature have been evaluated. The stress–strain curve for the PSF with 15% of the theoretical density is shown in Fig. 10a, while the optical image of a typical fracture surface is depicted in Fig. 10b. Each of the samples of PSF has exhibited mechanical behavior, slightly

Fig. 10 Mechanical behavior for (i) PSF; **a** stress–strain curve under compression, **b** optical micrograph of the fractured foam surface; (ii) For SSF **c** stress–strain curve under compression, **d** optical micrograph of the fractured foam surface

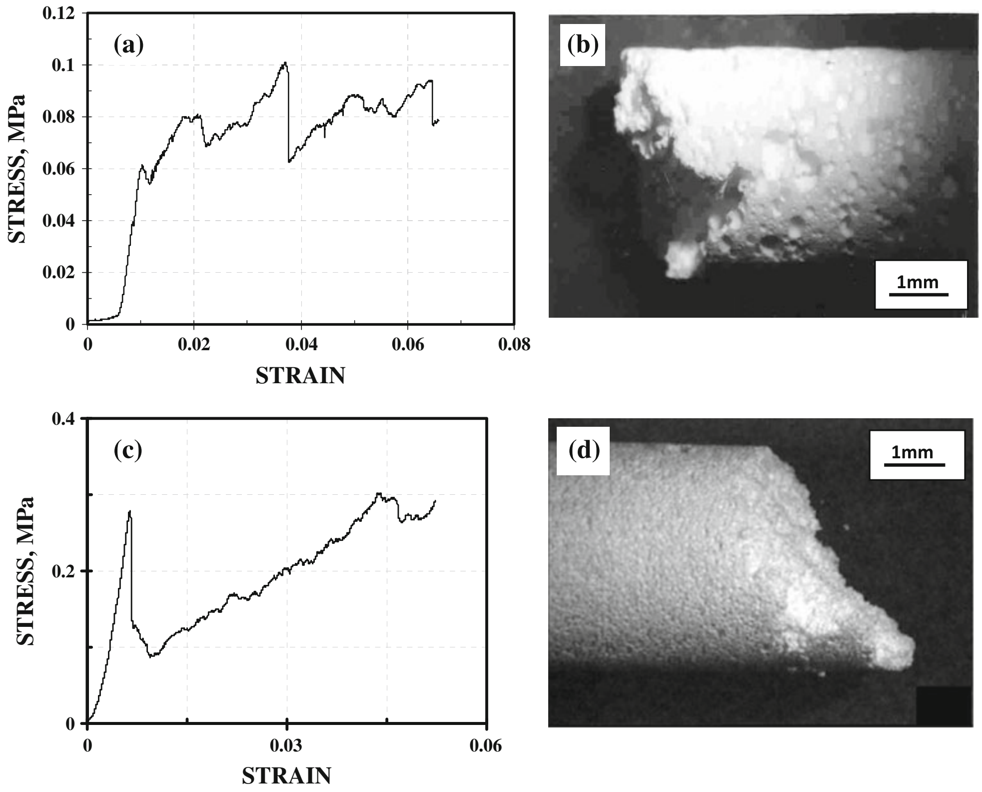

different from that of typical cellular materials. The compressive stress shows an initial linear elastic region, followed by a drop and subsequent rise. The stress–strain curve shows irregular cycles of rise and fall in stress with strain till the final complete failure occurs. The buckling and folding of struts, which are responsible for the support against compressive and shear loads [37], strongly influence the nature of stress–strain curves of foams till failure. Typically, as the struts or cell walls collapse under load, the stress is expected to fall. However, as the broken cell walls are squeezed so that these press against one another, there is an increase in the density of foam, leading to increase in the stress recorded in course of the compression test. As the strain is increased, the final failure of the foam occurs by shear, as is obvious from the angular relationship between the orientations of the fracture plane and compressive axis (Fig. 10a). The nature of the fracture surfaces is same for both the PSF and SSF compression samples.

Analysis of several stress–strain curves have led to average values of 0.1 and 17.46 MPa for the maximum compressive stress and Young's modulus, respectively. The Young's modulus and compressive strength of the PSF are only a third of those recorded for the SSF, as shown in Fig. 10c, d. The lower compressive strength of PSF than that of SSF can be attributed to the difference in the characteristics of their struts and cell wall densification. The difference in the quality of struts is confirmed on comparison of the SEM micrographs, as shown in Fig. 7c, f, respectively. The differences are: (i) the thickness of a randomly found strut in PSF is a half or one-third of those in SSF; (ii) the struts in PSF are poorly densified than that in SSF; and (iii) the cell walls in the PSF are porous, unlike those observed in case of SSF (Fig. 7b, e). In fact, the presence of fine pores in the cell walls of PSF contribute to such a wide variation of cell sizes in PSF.

The Weibull modulus for the compression test data of the PSF and SSF samples was calculated. It was observed that the PSF samples possess a very high Weibull modulus value of 9.2. The higher Weibull modulus of PSF than that of SSF is suggestive of the greater reliability of failure prediction in case of the former. A uniform and random distribution of cells as well as cell sizes and uniform strut thickness is expected to increase the Weibull modulus.

Comparison between PSF and SSF

cFor the purpose of comparison, the structure and mechanical properties of the PSF and SSF samples with almost similar relative densities are summarized in Table 2. The raw materials used for SSF and PSF are same, except for the presence of 10 vol% isopropanol in case of the latter foam. While the method and duration adopted for foaming were different, drying and sintering procedure were similar for PSF and SSF. Examination of the data presented in Table 2 leads to the following interesting inferences:

(i) While the suspension viscosity of PSF is lower than that of SSF, the drying shrinkages (linear as well as in volume) and mass loss are more in case of the former foam. This is suggestive of much higher liquid content in the wet PSF foams than in wet SSF.
(ii) Although cell counts are very close to each other, yet the cell size distribution appears different. There is a bimodal distribution in PSF with small (4–10 μm) as well as large cells (50–100 μm). On the other hand, the cell size distribution in the SSF shows a single peak at ≈5 μm, and variation between 50 and 250 μm.
(iii) The average density of PSF is more than that of SSF, in spite of a similar number of cells per unit length. This discrepancy is attributed to the presence of larger cells and wider cell size distribution in the SSF than in PSF.

Table 2 Comparison of the PSF and SSF

Properties	PSF	SSF
Suspension viscosity (Pa s)	<2	~3.4
Linear shrinkage (%)	11	4
Drying volume shrinkage (%)	28	23
Drying loss (of wt%)	40–50	12
Density (g/cc.)	0.344 ± 0.08	0.248 ± 0.03
Cell count (ppi)	8	10
Cell size distribution (μm)	Bimodal (4–10 and 50–100)	Monomodal (50–250)
Compression strength (MPa)	0.100	0.332
Young's modulus (MPa)	17.46	60
Weibull modulus	9.2	3.3
Porosity distribution	Random	Uniform
Strut thickness (μm)	2–3	5–6

(iv) The compressive strength and Young's modulus of the PSF are a third of that in SSF because of thinner and less densified struts in the former.

(v) The Weibull modulus of PSF samples has been found to be thrice that of SSF, indicating that a more uniform strut thickness and flaw size distribution exists in the former foams.

Summary and conclusions

A simple method for the preparation of porous silica through particle (PSF) and surfactant (SSF) stabilization of foams in the suspension has been developed. The method employs the use of partially hydrophobized silica powder particles for stabilization of foams at the air–water interphase. The air–water interfacial tension is reduced by the addition of isopropanol. The silica-based slurry composition with optimum solids loading and isopropanol (wetting agent) content has been determined for the best foaming conditions and particle stabilization.

The drying shrinkages in the PSF are found to be very high (28% in volume) as compared to SSF (23%), due to large water content of in the PSF foams. Increase in solids loading could be used to reduce the drying shrinkage. The optimization of this process allows the fabrication of sintered PSF panels of about 100 × 60 × 30 mm size and SSF panels of 100 × 100 × 25 mm size successfully. The silica foams processed using particle stabilization route have shown much reduced cell size than those found in foams prepared through long-chain surfactant based stabilization procedure. Such small cell size has resulted from the remarkable long-term stability achieved through the irreversible adsorption of colloidal particles at the air–water interface. Cell sizes within the range of 4 μm–1 mm (pore count 8 ppi) with nonuniform (random) porosity distribution have been achieved in the sintered PSF samples.

The silica foams produced using particle stabilization have compression strength and Young's modulus of 0.1 MPa and 17.46 MPa, respectively, each of which is almost a third of that present in the silica foams processed using surfactant stabilization. The PSF samples have shown higher Weibull modulus of 9.2, which is 3 times that ($m = 3.3$) obtained for SSF.

Acknowledgements The authors are thankful to Dr. M. Vijayakumar, DMRL, Hyderabad for his support. Also financial help from Defence Research and Development Organization (DRDO), INDIA, for carrying out this work is kindly acknowledged.

References

1. Sepulveda P (1997) Am Ceram Soc Bull 76:61
2. Scheffler M, Colombo P (2005) Cellular ceramics: structure, manufacturing, properties and applications. Wiley-VCH, UK
3. Woyansky JS, Scott CE, Minnear WP (1992) Am Ceram Soc Bull 71:1674
4. Saracco G, Montanaro L (1995) Ind Eng Chem Res 34:1471
5. Kim H, Lee S, Han Y, Park J (2006) J Mater Sci 41:6150. doi:10.1007/s10853-006-0574-x
6. Ruruta S, Katsuki H, Komarneni S (2001) J Porous Mater 8:43
7. Montanaro L, Jorand Y, Fantozzi G, Negro A (1998) J Eur Ceram Soc 18:1339
8. Hing KA (2005) Int J Ceram Technol 2:184
9. de sousa E, Rambo CR, Hotza D, de Oliveira APN, Fey T, Greil P (2008) Mater Sci Eng A 476:89
10. Fujiu T (1990) J Am Ceram Soc 73:85
11. Sepulveda P, Binner JGP (1999) J Eur Ceram Soc 19:2059
12. Gibson LJ, Ashby MF (1997) Cellular solids: structure and properties, 2nd edn. Cambridge University Press, UK
13. Carn F, Colin A, Achard M-F, Deleuze H, Saadi Z, Backov R (2004) Adv Mater 16:140
14. Gonzenbach UT, Studart AR, Tervoort E, Gauckler LJ (2007) J Am Ceram Soc 90:16
15. Du ZP, Bilbao-Montoya MP, Binks BP, Dickinson E, Ettelaie R, Murray BS (2003) Langmuir 19(8):3106
16. Dickinson E, Ettelaie R, Kostakis T, Murray BS (2004) Langmuir 20:8517
17. Binks BP, Horozov TS (2005) Angew Chem Int Ed 44:3722
18. Gonzenbach UT, Studart AR, Tervoort E, Gauckler LJ (2006) Angew Chem Int Ed 118:3606
19. Studart AR, Gonzenbach UT, Tervoort E, Gauckler LJ (2006) J Am Ceram Soc 89:1771
20. Carn F, Colin A, Pitois O, Adler M, Backov R (2009) Langmuir 25:7847
21. Carn F, Steunou N, Colin A, Livage J, Backov R (2005) Chem Mater 17:644
22. Wang HN, Yuan P, Zhou L, Guo YN, Zou J, Yu AM, Lu GQ, Yu CZ (2009) J Mater Sci 44:6484. doi:10.1007/s10853-009-3578-5
23. Carn F, Colin A, Achard MF, Deleuze H, Sanchez C, Backov R (2005) Adv Mater 17:62
24. Carn F, Achard M-F, Babot O, Deleuze H, Reculusa S, Backov R (2005) J Mater Chem 15:3887
25. Carn F, Derré A, Neri W, Babot O, Deleuze H, Backov R (2005) New J Chem 29:1346
26. Leroy CM, Carn F, Trinquecost M, Backov R, Delhaès P (2007) Carbon 45:2317
27. Backov R (2006) Soft Matter 2:452
28. Binks BP (2002) Curr Opin Colloid Interface Sci 7:21
29. Mishra S, Mitra R, Vijayakumar M (2008) J Eur Ceram Soc 28:1769
30. Mishra S, Mitra R, Vijayakumar M (2009) Mater Lett 63:2649
31. ASTM International (1999) C 577-99:99-102
32. Scheidegger AE (1974) The physics of flow through porous media, chap 4, 7. University of Toronto Press, Toronto, Canada
33. Carlos A, Leon LY (1998) Adv Colloid Interface Sci 76–77:341
34. Jena A, Gupta K (2002) Ceram Eng Sci Proc 23:277
35. Brezny R, Green DJ (1993) J Am Ceram Soc 76:2185
36. Maire E, Colombo P, Adrien J, Babout L, Biasetto L (2007) J Eur Ceram Soc 27:1973
37. Menges G, Knipschild F (1975) Polym Eng Sci 15:623